



## TdfH selectively binds metal-loaded tetrameric calprotectin for zinc import

Aloke K. Bera<sup>1</sup>, Runrun Wu<sup>2</sup>, Simone Harrison<sup>3</sup>, Cynthia Nau Cornelissen<sup>4</sup>, Walter J. Chazin<sup>3</sup>  & Nicholas Noinaj<sup>1,5</sup>  <sup>✉</sup>

To combat nutritional immunity, *N. gonorrhoeae* has evolved systems to hijack zinc and other metals directly from host metal-binding proteins such as calprotectin (CP). Here, we report the 6.1 Å cryoEM structure of the gonococcal surface receptor TdfH in complex with a zinc-bound CP tetramer. We further show that TdfH can also interact with CP in the presence of copper and manganese, but not with cobalt.

<sup>1</sup>Department of Biological Sciences, Purdue University, West Lafayette, IN 47907, USA. <sup>2</sup>Interdisciplinary Life Science - PULSe, Purdue University, West Lafayette, IN 47907, USA. <sup>3</sup>Departments of Biochemistry and Chemistry, and Center for Structural Biology, Vanderbilt University, Nashville, TN 37240, USA. <sup>4</sup>Center for Translational Immunology, Institute for Biomedical Sciences, Georgia State University, Atlanta, GA 30303, USA. <sup>5</sup>Purdue Institute for Inflammation, Immunology and Infectious Disease, Purdue University, West Lafayette, IN 47907, USA. ✉email: [nnoinaj@purdue.edu](mailto:nnoinaj@purdue.edu)

*Neisseria gonorrhoeae* causes the sexually transmitted infection gonorrhea, which can lead to more serious conditions including bacteremia, increased risk of HIV/AIDS, and infertility<sup>1,2</sup>. Due to the rapid emergence of multi-drug resistance, the CDC currently lists *N. gonorrhoeae* at the top of the list of urgent threats to human health, with treatment options now limited to just ceftriaxone. No vaccine option is currently available, intensifying the need for new, more effective antibiotics to combat *N. gonorrhoeae* infection. Recent approaches have targeted virulence factors found on the surface of the pathogen. These well-conserved membrane proteins facilitate pathogenesis by subverting nutritional immunity, which the host uses to combat the proliferation of bacterial invaders by limiting essential nutrients<sup>3–6</sup>. To counter this host defense, *N. gonorrhoeae* has evolved systems that specifically hijack nutrients from the host's nutritional immunity repertoire for their own survival<sup>7–9</sup>. One such example of this is the zinc transporter TdfH, which has recently been shown to pirate zinc from human calprotectin (CP) (Fig. 1a)<sup>10,11</sup>. CP is composed of two S100 EF-hand calcium-binding proteins, S100A8 and S100A9 that, uniquely among S100 proteins, greatly prefer to form their heterodimer over the

corresponding homodimers<sup>12</sup>. As a heterodimer, CP has two distinct transition metal-binding sites at the dimer interface<sup>3,13,14</sup>. Site 2 is a canonical S100 transition metal-binding site with three His and one Asp side chains that coordinates zinc and copper with high affinity. Site 1 is a unique transition metal-binding site composed of six His residues, which along with zinc and copper, is able to chelate Fe(II) and manganese<sup>14,15</sup>. Importantly, CP forms tetramers upon binding of calcium, zinc, copper, or manganese<sup>13,14</sup>. TdfH is a gonococcal TonB-dependent transporter that is zinc regulated and was recently shown to interact with human, but not mouse, CP through both zinc-binding sites<sup>16</sup>. However, the exact details of this TdfH-CP interaction, and the mechanism that enables TdfH to extract and import zinc, remain unknown since no structure that captures this interaction has yet been reported.

## Results and discussion

To better understand the requirements for TdfH to interact with human CP, TdfH containing an N-terminal twin-strep tag was expressed in inclusion bodies, refolded, and purified as described in our previous studies<sup>16</sup>. As a reference to monitor relative

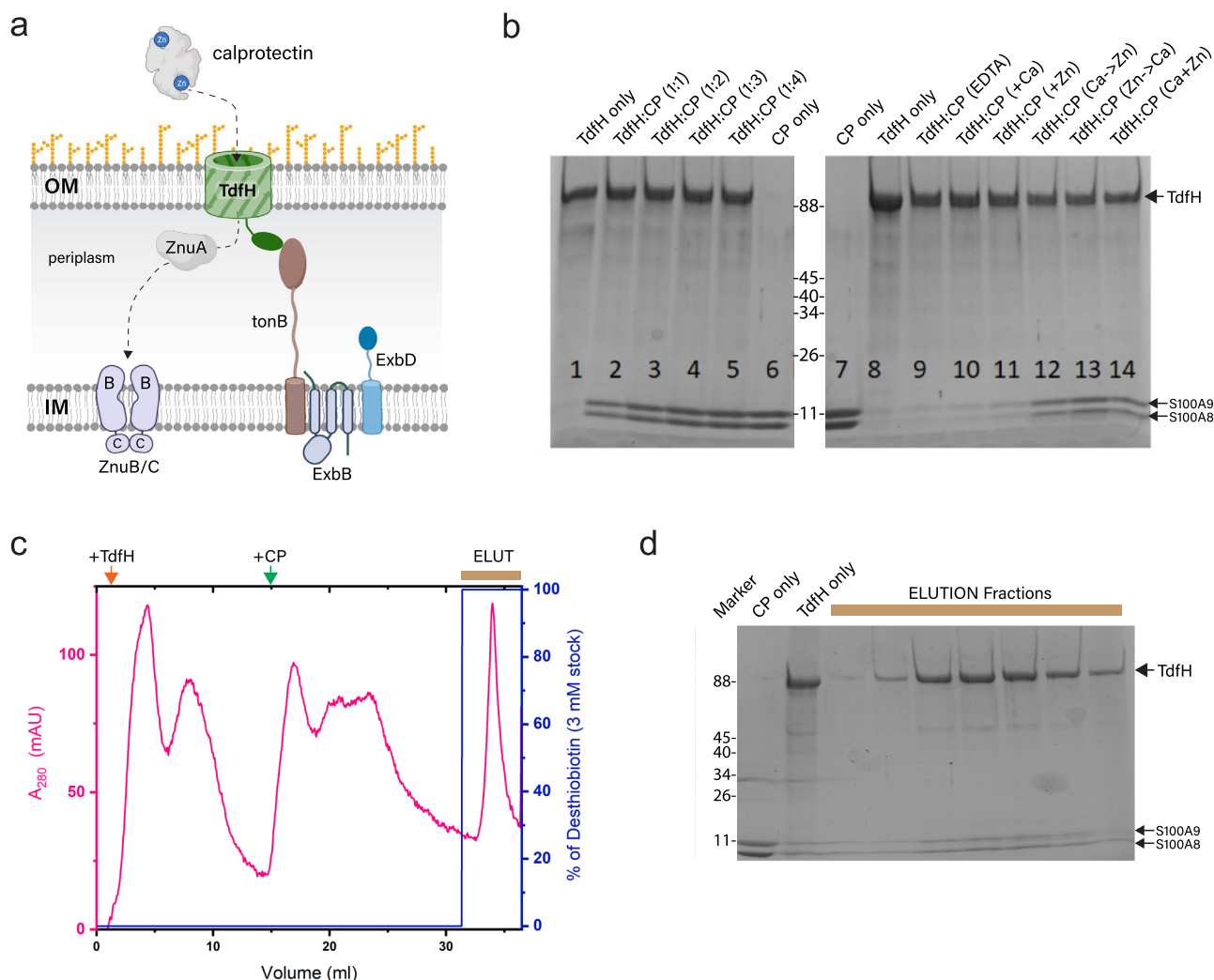


**Fig. 1 TdfH expression and complex formation for cryoEM studies.** **a** The role of TdfH in zinc piracy and import from calprotectin. Figure prepared using BioRender. **b** As a reference, purified TdfH and CP were loaded together with increasing concentrations of CP (lanes 1–6). Complex formation was then performed under various calcium and zinc conditions (lanes 8–14) and pulled down using Streptavidin MagneSphere Paramagnetic Particles. The eluted samples were then analyzed by SDS-PAGE analysis. CP is a heterodimer consisting of one copy each of S100A8 and S100A9. **c** Purification profile of complex formation on an Akta FLPC system using a StrepTactinXT column. TdfH was bound first, followed by CP, and lastly, the complex was eluted with desthiobiotin. **d** SDS-PAGE of the elution peak from panel **c**, verifying TdfH-CP complex formation.

binding ratios in our binding assays, TdfH was analyzed by SDS-PAGE with increasing ratiometric concentrations of CP (Fig. 1b; lanes 2–5). TdfH was then bound to Streptavidin MagneSphere Paramagnetic Particles and assayed for binding under various CP buffer conditions. No binding was observed with just calcium or zinc alone, or in the presence of EDTA (Fig. 1b; lanes 9–11). This was surprising since our earlier studies indicated that CP bound to TdfH without exogenous calcium or zinc<sup>16</sup>. We rationalize that because CP binds these metals with high affinity, residual metals may have been picked up from the buffer, enabling this interaction. Experiments reported here demonstrate that both calcium and zinc are required for the stable interaction between CP and TdfH and furthermore that the order of calcium or zinc addition to CP has no effect on the complex formation (Fig. 1b; lanes 12–14).

For cryoEM studies, TdfH from a large-scale prep was purified using a StrepTactinXT column attached to an Akta FPLC automated purification system. TdfH was first flowed over the column followed by CP, washing, and then elution of the complex (Fig. 1c). SDS-PAGE analysis confirmed the presence of both TdfH and CP (Fig. 1d) and the sample was then concentrated and grids were prepared. Data were collected using a Titan Krios equipped with an energy filter and a Gatan K3 detector. Particles were then picked and extracted from ~2,500 micrographs (Supplementary Fig. 1 and Table 1). Iterative rounds of 2D and 3D classification were used to filter particles, resulting in a final 3D

reconstruction of the TdfH-CP complex to 6.1 Å resolution using ~12,000 particles.

Inspection of the final map revealed that TdfH shared the same canonical fold as other TonB-dependent transporters, consisting of a 22-stranded β-barrel domain with an N-terminal plug (Fig. 2a, bottom). Additional density sitting above TdfH was initially modeled as a heterodimer of CP, however, a single heterodimer was insufficient to model the full density available. It was apparent, however, that there was pseudo-twofold symmetry which was consistent with a hetero-tetramer of CP. Therefore, we then performed a rigid fit of the crystal structure of hetero-tetrameric CP in complex with manganese (PDB ID 4XJK), consisting of two copies of the S100A8-S100A9 heterodimer (Fig. 2a, right). And while the resolution was not sufficient to allow unambiguous modeling of the full TdfH protein, it was clear that the TdfH loops extend up from the core barrel domain to mediate interaction with the CP tetramer. A homology model of TdfH<sup>16</sup> was then fit into the density and each of the extracellular loops manually adjusted to best fit the cryoEM density. The full structure was then refined in Phenix, producing model-to-map correlation coefficients of 0.69 for TdfH and ranging from 0.82–0.89 for the four chains of the CP tetramer (Supplementary Movie 1 and Table 1). The refined structure revealed that TdfH interacts with the CP tetramer through an interface involving site 1 of one CP heterodimer and site 2 of the other CP heterodimer (Fig. 2b). This demonstrates the requirement of both transition metal-binding sites for the interaction with TdfH and provides some corroboration for our previously reported binding studies which showed that CP mutants defective in zinc binding at site 1 and/or site 2 disrupted their interaction with TdfH<sup>16</sup>. Interestingly, the other two zinc sites of the CP tetramer do not appear to make direct contact with TdfH in our reconstruction. Efforts to improve the resolution of the TdfH-CP cryoEM structure have been hindered by the inability to saturate CP with zinc or other metals, as CP has a high propensity to precipitate out of solution before even achieving a 1:1 (metal:CP) ratio; a ratio of 2:1 would be needed to saturate both metal-binding sites. Our current studies suggest that this is mediated by intermolecular CP–CP interactions, which may require mutagenesis of surface residues to allow saturation of CP with zinc, and subsequently the formation of a more homogenous TdfH-CP complex for high-resolution structural characterization.

Upon discovering that TdfH directly interacts with the metal-binding sites of CP, we assayed the effect of other metals in mediating this interaction. We tested the ability of cobalt, copper, magnesium, and manganese to enable CP binding to TdfH and found that copper and manganese loaded CP could bind to TdfH; however, no interaction was detected between TdfH and CP when the latter was loaded with either cobalt or magnesium (Fig. 2c). While additional studies are needed, these data suggest that in addition to zinc, TdfH could play a role in the uptake of other essential transition metals including copper and manganese.

Our findings in the current study demonstrate that TdfH from *N. gonorrhoeae* selectively binds the zinc-loaded hetero-tetramer of CP, interacting simultaneously with both transition metal-binding sites. These binding properties would ensure the maximal yield of zinc from CP and optimally promote survival of *N. gonorrhoeae* within the human host during infection. We also show that TdfH can bind CP loaded with copper and manganese, hinting at a role for TdfH in the import of these, and possibly other, transition metals.

## Methods

**Expression and purification of CP and TdfH.** Calprotectin (CP) was prepared in the absence of calcium or zinc as previously reported and frozen in aliquots at –80 °C<sup>15,17</sup>. TdfH was expressed in inclusion bodies and refolded as described

**Table 1 CryoEM data collection and refinement statistics.**

	<b>NgTdfH-CP</b>
<b>Data collection and processing</b>	
Magnification	81,000
Voltage (kV)	300
Electron exposure (e <sup>-</sup> /Å <sup>2</sup> )	44.75
Defocus range (μm)	–1.5 to –2.5
Pixel size (Å)	0.54
Symmetry imposed	C1
Initial particles (Blob Picker) (no.)	2,587,376
Final particles (no.)	11,724
Map resolution (Å)	6.05
FSC threshold	0.143
<b>Refinement</b>	
Model Resolution (Å)	6.05
Map-model CC	
CC_mask	0.75
CC_box	0.71
CC_peaks	0.52
CC_volume	0.74
CC_TdfH only	0.69
CC_CP only	0.85
Model Composition	
Non-hydrogen atoms	8117
Protein residues	1115
B factors (Å <sup>2</sup> )	
Protein	190
R.M.S. deviations	
Bond lengths (Å)	0.007
Bond angles (°)	1.149
Validation	
MolProbity Score	3.11
Clashscore	52.49
Rotamer outliers (%)	1.54
Ramachandran Plot	
Favored (%)	77.36
Allowed (%)	22.18
Outliers (%)	0.46
EMDB code	EMD-25692

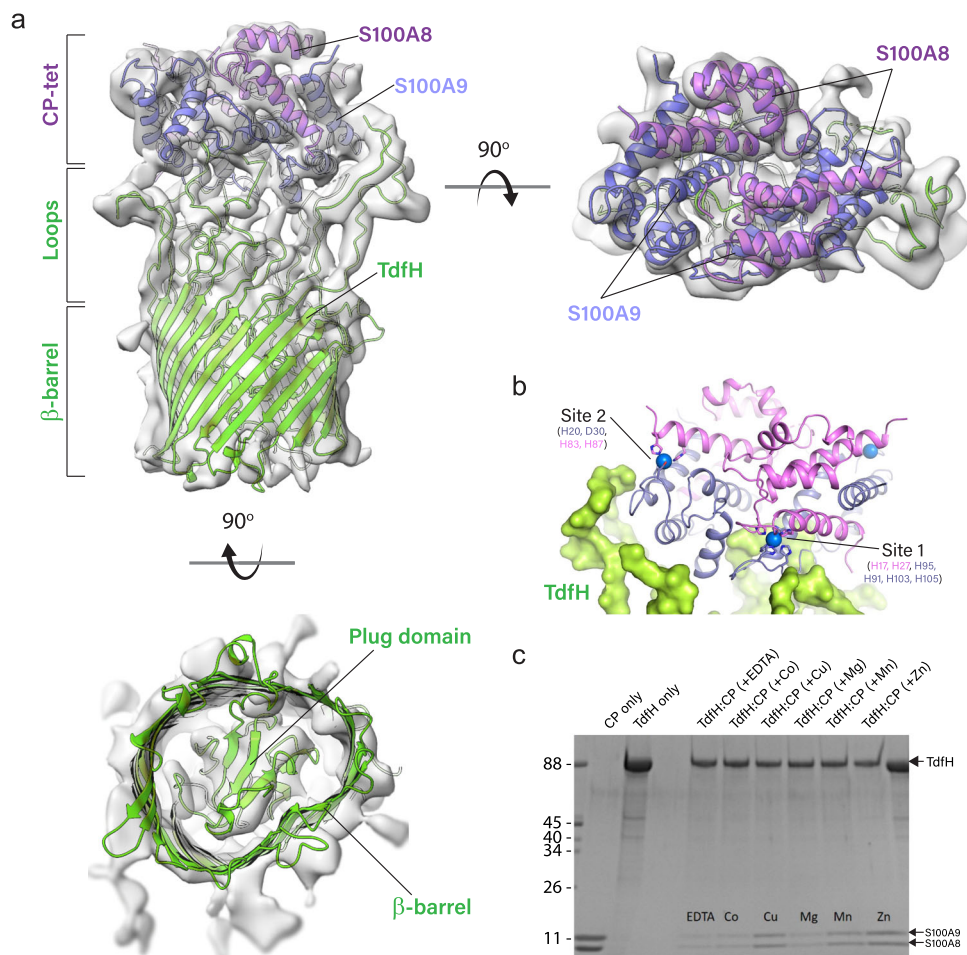


**Fig. 2 CryoEM structure of the TdfH-CP complex to 6.1 Å resolution.** **a** Orthogonal views of the cryoEM map aligned with the TdfH-CP complex structure (TdfH is in green, S100A8 in violet, and S100A9 in lavender). For clarity, calcium and zinc are not shown and the “surface dust” option in ChimeraX was used which removed most of the micelle density. **b** Zoomed view of the interaction of TdfH with site 1 and site 2 of CP, with zinc shown as blue spheres. For clarity, this view is rotated  $\sim 180^\circ$  compared to the view in panel **a** and calcium is not shown. **c** Pull-down assays demonstrate that TdfH is able to bind CP loaded with other metals such as copper (Cu) and manganese (Mn), but not with magnesium (Mg) or cobalt (Co).

previously with some modifications<sup>16</sup>. Briefly, the *tdfH* gene was subcloned into the pHis2 plasmid and expressed in BL21(DE3) cells, producing TdfH with an N-terminal 6x His-tag, TEV site, and twin-strep (TS) tags. The cells were harvested, lysed and the lysate was centrifuged at  $7000 \times g$  for 20 min at  $4^\circ\text{C}$  to spin down the inclusion bodies. The inclusion body pellet was washed three times with 1x PBS supplemented with 1% Triton X-100 and 5 mM ethylenediaminetetraacetic acid (EDTA) pH 7.4, one time with 3 M urea in 1x PBS, and two times with 1x PBS with 5 mM EDTA pH 7.4 using a dounce homogenizer.

To refold TdfH, washed inclusion bodies were resuspended to 5–10 mg/mL in 8 M urea containing 25 mM  $\beta$ -mercaptoethanol (BME) in a dounce homogenizer and supplemented with 0.5% sarkosyl. This was mixed for 15 min at room temperature and then centrifuged for 15 min at  $32,000 \times g$ . The supernatant was then diluted 60% in refolding buffer [20 mM Tris-HCl pH 8.0, 200 mM NaCl, 10% glycerol, and 0.17% *n*-Dodecyl- $\beta$ -*D*-Maltoside (DDM)] and dialyzed overnight at  $4^\circ\text{C}$  against a 20x volume of 1x PBS pH 7.4. The dialyzed sample was centrifuged at  $32,000 \times g$  for 15 mins at  $4^\circ\text{C}$  and further purified using immobilized metal affinity chromatography using a Ni-NTA column attached to an Atka Purifier (GE Healthcare). Peak fractions were verified by SDS-PAGE and the fractions containing TdfH were combined and the His-tag removed. TdfH was further purified using a Superdex 200 Increase 10/300 GL column (GE Healthcare) in 1x PBS, pH 7.4, 0.02% lauryl maltose neopentyl glycol (LMNG).

**Small-scale pull-down assays measuring CP binding to TdfH.** To determine the optimal conditions for complex formation, TdfH in 1x PBS, pH 7.4, 0.02% LMNG was first bound to Streptavidin MagneSphere Paramagnetic Particles (Promega) and washed in 1x PBS, pH 7.4, 0.02% LMNG. CP was then added under the following conditions: (i) 5 mM EDTA (ii) 200  $\mu\text{M}$   $\text{CaCl}_2$ , (iii) 10  $\mu\text{M}$   $\text{ZnCl}_2$ , (iv) incubated first with 200  $\mu\text{M}$   $\text{CaCl}_2$ , then with 10  $\mu\text{M}$   $\text{ZnCl}_2$ , (v) incubated first with 10  $\mu\text{M}$   $\text{ZnCl}_2$ , then with 200  $\mu\text{M}$   $\text{CaCl}_2$ , and (vi) simultaneously with 10  $\mu\text{M}$   $\text{ZnCl}_2$

and 200  $\mu\text{M}$   $\text{CaCl}_2$ . Lastly, the particles were washed, then the complexes were eluted with 50 mM biotin and analyzed by SDS-PAGE.

**Large-scale complex formation of TdfH-CP for cryoEM.** For large-scale complex formation, refolded TdfH in 1x PBS, pH 7.4, 0.02% LMNG was applied and the flowthrough reapplied to a 1 mL StrepTactinXT (IBA Lifesciences) column attached to an Akta FPLC automated purification system (GE Healthcare). The column was washed and then CP (preincubated with  $\text{CaCl}_2$  and  $\text{ZnCl}_2$ ) was applied and the flowthrough reapplied 2x, the column was washed again, and then the complex was eluted using sample buffer supplemented with 3 mM desthiobiotin and the fractions analyzed by SDS-PAGE. Fractions containing the TdfH-CP complex were then pooled and concentrated to  $\sim 4$  mg/mL. One limiting factor of this study is our inability to fully saturate CP with zinc, something that became obvious during our cryoEM studies. CP has a high propensity to precipitate out of solution before even reaching a 1:1 (zinc:CP) ratio; a ratio of 2:1 would be needed to fully saturate CP. From analysis of our cryoEM results, this leads to heterogeneity of the complex and limits the number of zinc saturated TdfH-CP particles that can be analyzed.

**CryoEM data acquisition, analysis, and image processing.** For grid preparation, the TdfH-CP complex (1.5–3 mg/mL) was applied to glow-discharged (Easiglow, Pelco) Quantifoil R 3.5/1 Cu-200 mesh grids and plunge frozen using a Thermo Scientific Vitrobox Mark IV. The cryoEM data were collected on a Titan Krios microscope (ThermoFisher) operated at 300 kV with a nominal magnification of 81,000x using a K3 direct electron detector (Gatan) operated in super-resolution counting mode using Leginon for automated data collection. The images were recorded at a defocus range of  $-1.5$  to  $-2.5$   $\mu\text{m}$ , with a calibrated physical pixel size of 0.54 Å/pixel, with a total dose of 44.75  $\text{e}^-/\text{Å}^2$ ; a total of  $\sim 3300$  movies were collected.



For image processing, motion correction of the movies was conducted on the fly using MotionCor2<sup>18</sup> with a binning factor of 2 implemented within RELION-3<sup>19</sup>. Using Cryosparc<sup>20</sup>, images were filtered based on CTF-resolution fit, leaving ~2500 images for initial blob picking. Initial templates were prepared by iterative rounds of 2D classification, which were then used for template picking, producing an initial ~2.5 million particles. Further filtering by interactive rounds of 2D classification yielded ~120,000 particles of top and side views, based on clear features including the presence of the detergent micelle. Multiple 3D classes were prepared by ab initio modeling followed by heterogeneous refinement, with only a single 3D class (~63,000 particles) having features consistent with a membrane protein complex within a detergent micelle. The 3D classification was iterated to further filter the particles until a homogenous 3D class was attained. Homogenous refinement was then performed, followed by non-uniform refinement and finally, local refinement to produce the final 6.1 Å reconstruction of the TdfH-CP complex. During the 3D classification, a majority of the particles appeared to be TdfH-only; however, attempts to process these further was unsuccessful due to heterogeneity of the shape of the barrel and the lack of defined features outside of the micelle. We hypothesize that this may be due to the increased flexibility of the barrel and loops of TdfH in the absence of CP.

For model building, the manganese-bound CP structure (PDB ID 4GGF) and our previously reported homology model for TdfH<sup>16</sup> were fit into the map using ChimeraX<sup>21</sup>. For TdfH, the loops were all removed and manually traced into the visible density available. Given the resolution and lack of sufficient density, not all residues were modeled, which is consistent with other similar structures where many of the large extracellular loops are expected to be partially or fully disordered due to flexibility. The final model was refined using real-space refinement, concurrently performing rigid-body refinement of all the individual chains with secondary structure restraints. All model building was performed using COOT<sup>22</sup> and real-space refinement was performed using PHENIX<sup>23</sup>. A higher resolution cryoEM structure is needed to unambiguously localize all of the residues of TdfH.

**Small-scale pull-down assays measuring the effect of metals on CP binding to TdfH.** To determine the effect of metals other than zinc on complex formation between CP and TdfH, TdfH in 1x PBS, pH 7.4, 0.02% LMNG was first bound to Streptavidin MagneSphere Paramagnetic Particles (Promega) and washed in 1x PBS, pH 7.4, 0.02% LMNG. CP was then added under the following conditions: (i) 5 mM EDTA, (ii) 200 μM CaCl<sub>2</sub> and 10 μM of CoCl<sub>2</sub>, (iii) 200 μM CaCl<sub>2</sub> and 10 μM of CuCl<sub>2</sub>, (iv) 200 μM CaCl<sub>2</sub> and 10 μM of MgCl<sub>2</sub>, (v) 200 μM CaCl<sub>2</sub> and 10 μM of MnCl<sub>2</sub>, and (vi) 200 μM CaCl<sub>2</sub> and 10 μM of ZnCl<sub>2</sub>. Lastly, the particles were washed, then the complexes were eluted with 50 mM biotin and analyzed by SDS-PAGE.

**Reporting summary.** Further information on research design is available in the Nature Research Reporting Summary linked to this article.

## Data availability

The cryoEM map of the TdfH-CP complex has been deposited in the Electron Microscopy Data Bank with accession EMDB code EMD-25692. All other data are available from the authors on request.

Received: 27 June 2021; Accepted: 6 January 2022;

Published online: 31 January 2022

## References

- Sparling, P. et al. in *Sexually Transmitted Diseases* (eds Wasserheit, J. N. et al.) (McGraw-Hill, 2008).
- Frieden, T. *Antibiotic Resistance Threats in the United States* (DIANE Publishing Company, 2013).
- Zackular, J. P., Chazin, W. J. & Skaar, E. P. Nutritional immunity: S100 proteins at the host-pathogen interface. *J. Biol. Chem.* **290**, 18991–18998 (2015).
- Weinberg, E. D. Human lactoferrin: a novel therapeutic with broad spectrum potential. *J. Pharm. Pharmacol.* **53**, 1303–1310 (2001).
- Miethke, M. & Skaar, A. Neutrophil gelatinase-associated lipocalin expresses antimicrobial activity by interfering with L-norepinephrine-mediated bacterial iron acquisition. *Antimicrob. Agents Chemother.* **54**, 1580–1589 (2010).
- Hood, M. I. & Skaar, E. P. Nutritional immunity: transition metals at the pathogen-host interface. *Nat. Rev. Microbiol.* **10**, 525–537 (2012).
- Stork, M. et al. Zinc piracy as a mechanism of *Neisseria meningitidis* for evasion of nutritional immunity. *PLoS Pathogens* **9**, e1003733 (2013).
- Neumann, W., Hadley, R. C. & Nolan, E. M. Transition metals at the host-pathogen interface: how *Neisseria* exploit human metalloproteins for acquiring iron and zinc. *Essays Biochem.* **61**, 211–223 (2017).
- Yadav, R. et al. Structural basis for evasion of nutritional immunity by the pathogenic *Neisseriae*. *Front. Microbiol.* **10**, 2981 (2019).
- Hagen, T. A. & Cornelissen, C. N. *Neisseria gonorrhoeae* requires expression of TonB and the putative transporter TdfF to replicate within cervical epithelial cells. *Mol. Microbiol.* **62**, 1144–1157 (2006).
- Jean, S., Juneau, R. A., Criss, A. K. & Cornelissen, C. N. *Neisseria gonorrhoeae* evades calprotectin-mediated nutritional immunity and survives neutrophil extracellular traps by production of TdfH. *Infect. Immun.* **84**, 2982–2994 (2016).
- Hunter, M. J. & Chazin, W. J. High level expression and dimer characterization of the S100 EF-hand proteins, migration inhibitory factor-related proteins 8 and 14. *J. Biol. Chem.* **273**, 12427–12435 (1998).
- Korndorfer, I. P., Brueckner, F. & Skerra, A. The crystal structure of the human (S100A8/S100A9)<sub>2</sub> heterotetramer, calprotectin, illustrates how conformational changes of interacting alpha-helices can determine specific association of two EF-hand proteins. *J. Mol. Biol.* **370**, 887–898 (2007).
- Gagnon, D. M. et al. Manganese binding properties of human calprotectin under conditions of high and low calcium: X-ray crystallographic and advanced electron paramagnetic resonance spectroscopic analysis. *J. Am. Chem. Soc.* **137**, 3004–3016 (2015).
- Damo, S. M. et al. Molecular basis for manganese sequestration by calprotectin and roles in the innate immune response to invading bacterial pathogens. *Proc. Natl Acad. Sci. USA* **110**, 3841–3846 (2013).
- Kammermer, M. T. et al. Molecular insight into TdfH-mediated zinc piracy from human calprotectin by *Neisseria gonorrhoeae*. *mBio* <https://doi.org/10.1128/mBio.00949-20> (2020).
- Kehl-Fie, T. E. et al. Nutrient metal sequestration by calprotectin inhibits bacterial superoxide defense, enhancing neutrophil killing of *Staphylococcus aureus*. *Cell Host Microbe* **10**, 158–164 (2011).
- Zheng, S. Q. et al. MotionCor2: anisotropic correction of beam-induced motion for improved cryo-electron microscopy. *Nat. Methods* **14**, 331–332 (2017).
- Scheres, S. H. RELION: implementation of a Bayesian approach to cryo-EM structure determination. *J. Struct. Biol.* **180**, 519–530 (2012).
- Punjani, A., Rubinstein, J. L., Fleet, D. J. & Brubaker, M. A. cryoSPARC: algorithms for rapid unsupervised cryo-EM structure determination. *Nat. Methods* **14**, 290–296 (2017).
- Pettersen, E. F. et al. UCSF ChimeraX: structure visualization for researchers, educators, and developers. *Protein Sci.* **30**, 70–82 (2021).
- Emsley, P., Lohkamp, B., Scott, W. G. & Cowtan, K. Features and development of Coot. *Acta Crystallogr. Sect. D Biol. Crystallogr.* **66**, 486–501 (2010).
- Adams, P. D. et al. PHENIX: a comprehensive Python-based system for macromolecular structure solution. *Acta Crystallogr. Sect. D Biol. Crystallogr.* **66**, 213–221 (2010).

## Acknowledgements

We thank members of the Noinaj and Cornelissen laboratories for helpful comments on the studies and critical reading of the manuscript. We thank Dr. Thomas Klose (Purdue CryoEM Facility) for his assistance with the collection of the cryoEM data. These studies were funded by NIH grants R01AI127793 and U19AI144182 (CNC). The cryoEM studies were funded, in part, with support from the Indiana Clinical and Translational Sciences Institute funded, in part by Grant Number UL1TR002529 from the NIH, National Center for Advancing Translational Sciences, Clinical and Translational Sciences Award.

## Author contributions

AB expressed and purified the TdfH and prepared the complex. AB also performed the binding studies in the presence of different metal compositions. SH and WJC provided the calprotectin. RW collected the cryoEM data for the TdfH/calprotectin complex. NN performed the cryoEM reconstruction. CNC, WJC, and NN conceived the project and wrote the manuscript.

## Competing interests

The authors declare no competing interests.

## Additional information

**Supplementary information** The online version contains supplementary material available at <https://doi.org/10.1038/s42003-022-03039-y>.

**Correspondence** and requests for materials should be addressed to Nicholas Noinaj.

**Peer review information** *Communications Biology* thanks the anonymous reviewers for their contribution to the peer review of this work. Primary Handling Editors: Ingrid Span and Anam Akhtar.

**Reprints and permission information** is available at <http://www.nature.com/reprints>

**Publisher's note** Springer Nature remains neutral with regard to jurisdictional claims in published maps and institutional affiliations.



**Open Access** This article is licensed under a Creative Commons Attribution 4.0 International License, which permits use, sharing, adaptation, distribution and reproduction in any medium or format, as long as you give appropriate credit to the original author(s) and the source, provide a link to the Creative Commons license, and indicate if changes were made. The images or other third party material in this article are included in the article's Creative Commons license, unless indicated otherwise in a credit line to the material. If material is not included in the article's Creative Commons license and your intended use is not permitted by statutory regulation or exceeds the permitted use, you will need to obtain permission directly from the copyright holder. To view a copy of this license, visit <http://creativecommons.org/licenses/by/4.0/>.

© The Author(s) 2022